IVYSPRING INTERNATIONAL PUBLISHER

Theranostics

2017; 7(14): 3527-3538. doi: 10.7150/thno.19422

Research Paper

The Role of Nitric Oxide during Sonoreperfusion of Microvascular Obstruction

Francois T.H. Yu[1], Xucai Chen[1], Adam C. Straub[2] and John J. Pacella[1]✉

1. Center for Ultrasound and Molecular Imaging and Therapeutics, University of Pittsburgh School of Medicine, Pittsburgh, Pennsylvania, USA,
2. Vascular Medicine Institute, University of Pittsburgh School of Medicine, Pittsburgh, Pennsylvania, USA.

✉ Corresponding author: John J. Pacella, MS, MD, FACC, Associate Professor of Medicine, University of Pittsburgh School of Medicine, 200 Lothrop Street, Pittsburgh, PA 15213; Phone: 412-647-5840; Fax: 412-647-4227; E-mail: pacellajj@upmc.edu

Received: 2017.01.31; Accepted: 2017.07.10; Published: 2017.08.18

Abstract

Rationale: Microembolization during PCI for acute myocardial infarction can cause microvascular obstruction **(MVO)**. MVO severely limits the success of reperfusion therapies, is associated with additional myonecrosis, and is linked to worse prognosis, including death. We have shown, both in *in vitro* and *in vivo* models, that ultrasound **(US)** and microbubble **(MB)** therapy (termed "sonoreperfusion" or "**SRP**") is a theranostic approach that relieves MVO and restores perfusion, but the underlying mechanisms remain to be established.

Objective: In this study, we investigated the role of nitric oxide (**NO**) during SRP.

Methods and results: We first demonstrated in plated cells that US-stimulated MB oscillations induced a 6-fold increase in endothelial nitric oxide synthase **(eNOS)** phosphorylation *in vitro*. We then monitored the kinetics of intramuscular NO and perfusion flow rate responses following 2-min of SRP therapy in the rat hindlimb muscle, with and without blockade of eNOS with LNAME. Following SRP, we found that starting at 6 minutes, intramuscular NO increased significantly over 30 min and was higher than baseline after 13 min. Concomitant contrast enhanced burst reperfusion imaging confirmed that there was a marked increase in perfusion flow rate at 6 and 10 min post SRP compared to baseline (>2.5 fold). The increases in intramuscular NO and perfusion rate were blunted with LNAME. Finally, we tested the hypothesis that NO plays a role in SRP by assessing reperfusion efficacy in a previously described rat hindlimb model of MVO during blockade of eNOS. After US treatment 1, microvascular blood volume was restored to baseline in the MB+US group, but remained low in the LNAME group. Perfusion rates increased in the MB+US group after US treatment 2 but not in the MB+US+LNAME group.

Conclusions: These data strongly support that MB oscillations can activate the eNOS pathway leading to increased blood perfusion and that NO plays a significant role in SRP efficacy.

Key words: Microvascular obstruction, ultrasound, microbubbles, sonothrombolysis, nitric oxide

Introduction

Cardiovascular disease accounts for 30% of deaths globally, and of these, nearly one-half are due to coronary heart disease (**CHD**) [1] with acute myocardial infarction (**AMI**) occurring every 44 seconds [1] in the United States. Current therapy for AMI hinges on immediately restoring epicardial coronary artery patency with percutaneous coronary intervention (**PCI**), such as with primary stenting. However, even after recanalization of the epicardial artery, there is a failure of microvascular perfusion in many patients due to microvascular obstruction (**MVO**)[2]. Even in patients with angiographically restored epicardial coronary artery flow, MVO incidence varies between 17% [3] to over 80% [4]. MVO severely limits the success of reperfusion therapies [5-9], is associated with additional

myonecrosis, and is linked to worse prognosis, including death [2, 10, 11]. Mechanical obstruction by embolized and *in situ* microvascular thrombi [12] is a major component of MVO; other observations include microvascular spasm, myocardial edema, platelet aggregation, and leukocyte plugging. PCI itself causes microembolization of atherothrombotic material from the stented site of plaque rupture into the microcirculation of the infarct bed [13], accounting for a significant portion of MVO after PCI [14], conferring adverse prognosis [12], and thus suggesting the need for therapies directed against MVO.

We have previously reported successful reperfusion of MVO by insonifying lipid microbubbles (**MB**) within the obstructed microvascular bed using long tone burst ultrasound (**US**) (termed sonoreperfusion, or "**SRP**") in a rat hindlimb model of MVO [15]. This theranostic approach, by which MVO can be treated and perfusion characterized using the same acoustic modality, has been shown to successfully restore microvascular flow *in vitro* [16] and *in vivo* [15] but the mechanisms remain largely unknown. Although there is evidence that the physical effects of microbubbles (MB) oscillations can mechanically disrupt thrombus in SRP therapy [17], we wondered if MB oscillations may have other bioeffects, notably on the vascular endothelium.

We hypothesized that ultrasound-induced MB oscillations in the microcirculation impart shear stress on the surrounding medium [18], causing endothelial mechanotransduction and Nitric Oxide (**NO**) release. Indeed, the important role of endothelial NO in modulating vasomotor tone is well established and has been studied extensively since the seminal work of Furchgott et al in 1980 [19]. NO is not only a potent vasodilator, but also reverses numerous additional pathologic components of MVO [20] to augment microvascular perfusion, such as platelet aggregation, increased adhesion of inflammatory cells, and edema, potentially lending multifactorial therapeutic mechanisms to the US-MB interaction. The effect of using long tone bursts US-induced MB oscillations at 1 MHz occurring with our SRP therapy for MVO on endothelial NO release is unknown.

Accordingly, in the present study, we investigated the contribution of NO to SRP in a series of experiments to determine if: (1) SRP can cause endothelial NO phosphorylation in cultured endothelial cells; (2) SRP can increase intramuscular NO in an intact hindlimb and cause changes in microvascular perfusion kinetics; (3) NO is implicated in SRP efficacy by blocking endothelial NO with N-Nitro-L-Arginine Methyl Ester (**LNAME**) prior to SRP therapy in a rat model of MVO.

Methods

Ultrasound contrast agents

For therapy, phospholipid-encapsulated MB containing perfluorocarbon gas (Perfluorobutane, Fluoromed, Round Rock, TX) were prepared in house and measured by electrozone sensing using a 50 µm aperture (Multisizer 3, Beckham Coulter, Brea, CA) [21]. In brief, 1,2-distearoyl-sn-glycero-3-phosphocholine (Avanti Polar Lipids Inc., Alabaster, AL), polyoxyethylene(40)stearate (Sigma Aldrich, St Louis, MO) and 1,2-distearoyl-sn-glycero-3-phosphoethanolamine-N-[methoxy(polyethylene glycol)-2000] (Avanti Polar Lipids) were mixed in chloroform in 88:11:1 molar ratios, dried under a stream of argon gas and stored under vacuum overnight. The film was rehydrated in 4 mL saline in a glass vial filled with an overhead of PFC. The lipids and PFC were sonicated for 75 s (XL2020, Qsonica LLC, Newtown, CT) and the resulting MB were washed 3 times in saline, yielding therapy microbubbles with a diameter of 3.5 ± 1.1 µm in diameter (Multisizer 3, Beckman Coulter) and were stored in sealed glass vials filled with PFC until usage (within 2 weeks of fabrication). Definity microbubbles (Lantheus Medical Imaging, North Billerica, MA) were used for contrast perfusion imaging. These MBs have a mean size of 1.1-3.3 µm and concentration of 1.2×10^{10} MB/mL and were administered via jugular access at a flow rate of 2 mL/h.

In vitro eNOS phosphorylation

Human umbilical vein endothelial cells (HUVEC #C2519A, passage <10, Lonza, Basel, Switzerland) were cultured in EGM media (Lonza) to 100% confluence (~500,000 cells) in petri dishes (Pall corporation, Port Washington, NY), pre-coated with fibronectin (1.6 µg/mL, Sigma Aldrich) (Figure 1).

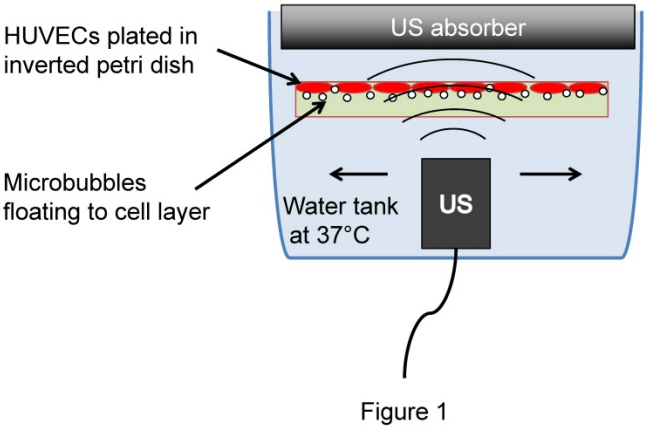

Figure 1

Figure 1: Cell culture experimental setup for *in vitro* exposure of HUVECs to microbubbles and ultrasound.

Cells were then incubated for 10 min (37°, 5% CO_2) in the presence of phosphatase inhibitor (Halt, Thermo Fisher Scientific) before filling up the plate with media (M199, Lonza) supplemented with 2% fetal bovine serum (Atlanta Biologicals, Flowery Branch, GA) containing therapeutic microbubbles (3×10^7 MB/plate). The plates were then covered, inverted and incubated upside down for 10 min to allow MB to float to the cell layer. The plate was then transferred upside down into a water bath and sonicated for 2 min (1 MHz, 5,000 cycles, PRF 100 Hz, 100 kPa). In some wells, a calcium ionophore (Ionomycin 2 μM, Sigma) was added to induce eNOS phosphorylation for positive control. All cells were collected 7 min after treatment and processed for Western blotting analysis. Proteins were run on 8% SDS-page gel and transferred onto polyvinylidene difluoride membranes (EMD Millipore, Billerica, MA). Purified mouse anti-human-eNOS (pS1177, #612392, BD Transduction Laboratories) was used for the detection of phosphorylated eNOS (p-eNOS). Purified mouse anti-human-eNOS/NOS type III (#610296, BD Transduction Laboratories) was used for the detection of total eNOS (t-eNOS). For immunostaining, cells were fixed in 4% paraformaldehyde and incubated with purified mouse anti-human-eNOS (pS1177, #612392, BD Transduction Laboratories), and visualized using AlexaFluor 488 goat anti-mouse IgG (Invitrogen) after counterstained with Hoechst 33342 (Thermo Fisher).

Cell viability assay

Following MB+US exposure, culture plates (n=3/group) were analyzed for cell viability. Because MB+US can cause cell detachment, cells in the supernatant were spun down and collected. Plated cells were trypsinized and collected. Cells were then exposed to 0.2% Trypan blue and counted on a hemocytometer. Three samples were analyzed per group and each sample was counted in triplicates.

Cell metabolic activity

Following MB+US exposure, the media was replaced with EGM and incubated for 24 h to allow cell recovery. The next day, cells were exposed to Alamar Blue (ThermoFisher) for 1 h and the supernatant fluorescence at (535/595 nm) was measured using a plate reader (Beckman Coulter). Background absorbance from plates without cells was subtracted from the measurement and normalized to the absorbance from the 'No treatment' group.

Microthrombi Preparation

Microthrombi were created by recalcification of citrated porcine blood and mechanical disruption by forcing through needles of decreasing diameters, followed by filtration through a 200 μm pore mesh. Details and characterization can be found in supplemental methods (Figure S1).

Animal preparation

All animal studies were approved by the Institutional Animal Care and Use Committee at the University of Pittsburgh. We used our previously developed rodent hindlimb model [15], to induce microvascular occlusion of the hindlimb gastrocnemius muscle. In rats weighing 262 ± 35 g, we induced anesthesia by inhalation of isoflurane (2.5%) and inserted an arterial cannula (PE-10, Becton Dickinson) via contralateral femoral access and advanced it to the abdominal aorta for the direct injection of microthrombi and therapeutic MB into the left hindlimb (Figure 2A) in order to achieve first pass MB delivery. An angiocatheter (24G, ¾ inch long) was placed in the right internal jugular vein for infusion of Definity microbubbles (Lantheus Medical Imaging) for contrast imaging. The jugular venous catheter was also used for administration of LNAME (10 mg/kg, Sigma-Aldrich).

Ultrasound Therapy and Perfusion Imaging

A 1 MHz single element transducer (A303S, ½ inch, Olympus NDT, Waltham, MA) was used for therapeutic US delivery, positioned vertically above the hindlimb, and coupled to the shaved skin using acoustic gel. The alignment was verified by visualization of the destruction of microbubbles in the central area of the image by the therapeutic pulse. The therapeutic transducer was previously calibrated in a degassed water tank using a lipstick hydrophone (HGL-0200, Onda Corporation, Sunnyvale, CA). The therapeutic pulse comprised US tone bursts 5,000 cycles in duration delivered every 3 seconds at a peak negative pressure of 1.5 MPa. Perfusion imaging was performed with a clinical scanner (Siemens, Sequoia, 15L8 probe) during continuous infusion (via right internal jugular vein) of Definity microbubbles (2 mL/h). The syringe containing the MB was rotated continuously to avoid MB floatation. The imaging probe was positioned horizontally with respect to the hindlimb and in a plane perpendicular to the therapy transducer beam to view the hindlimb in the longitudinal plane, such that the femoral bone was located in the upper right side of the image and the major feeding vessels could be observed, with blood flow traversing from right to left. The US therapeutic beam pattern and positioning respective to the imaging plane is shown in supplemental Figure S2. Imaging was performed in contrast pulse sequence mode (**CPS**) at 7 MHz, at an imaging mechanical

index (MI) of 0.2 and a framerate of 5 Hz. The imaging probe was used to deliver a burst pulse (5 frames at an MI of 1.9), which cleared the MB from the field of view. Perfusion kinetics was then tracked as the MB replenished the vascular network, and the cine loops were stored for offline processing. The dynamic range (60 dB), digital gain (0 dB), scanner compression curve (linear), along with other image processing parameters were fixed.

Image Analysis

Image analysis was performed offline on the cine loops obtained in CPS mode using custom Matlab software using an approach previously described [22] and are summarized in supplemental methods.

Experimental protocol for intramuscular NO and perfusion kinetics following SRP

A catheter probe (amiNO-IV, Innovative Instruments Inc, Tampa, FL) was calibrated following the manufacturer instructions and placed intramuscularly in the hindlimb in the area to be treated with therapeutic US in 4 animals. The probe was then left to equilibrate for 30 min to 1 h until the signal stabilized. Therapeutic US (5,000 cycles every 3 s at 1 MHz, 1.5 MPa) was delivered during simultaneous infusion of our custom lipid MB into the femoral artery catheter via syringe pump at a flow rate of 3 mL/h. Therapeutic SRP was given for 2 min. Intramuscular NO levels were monitored continuously and microvascular tissue perfusion kinetics were monitored by contrast ultrasound at baseline, post US, and at 3, 6, 10 and 30 min post US. L-NAME (10 mg/kg iv) was then administered to block endothelial nitric oxide production. Five minutes post LNAME, SRP therapy was repeated for 2 min in the same animal without moving the instrumentation. NO measurements were normalized to pre-SRP values. Burst replenishment imaging was performed again at baseline, post US and at 3, 6, 10 and 30 min post US (Figure 2B).

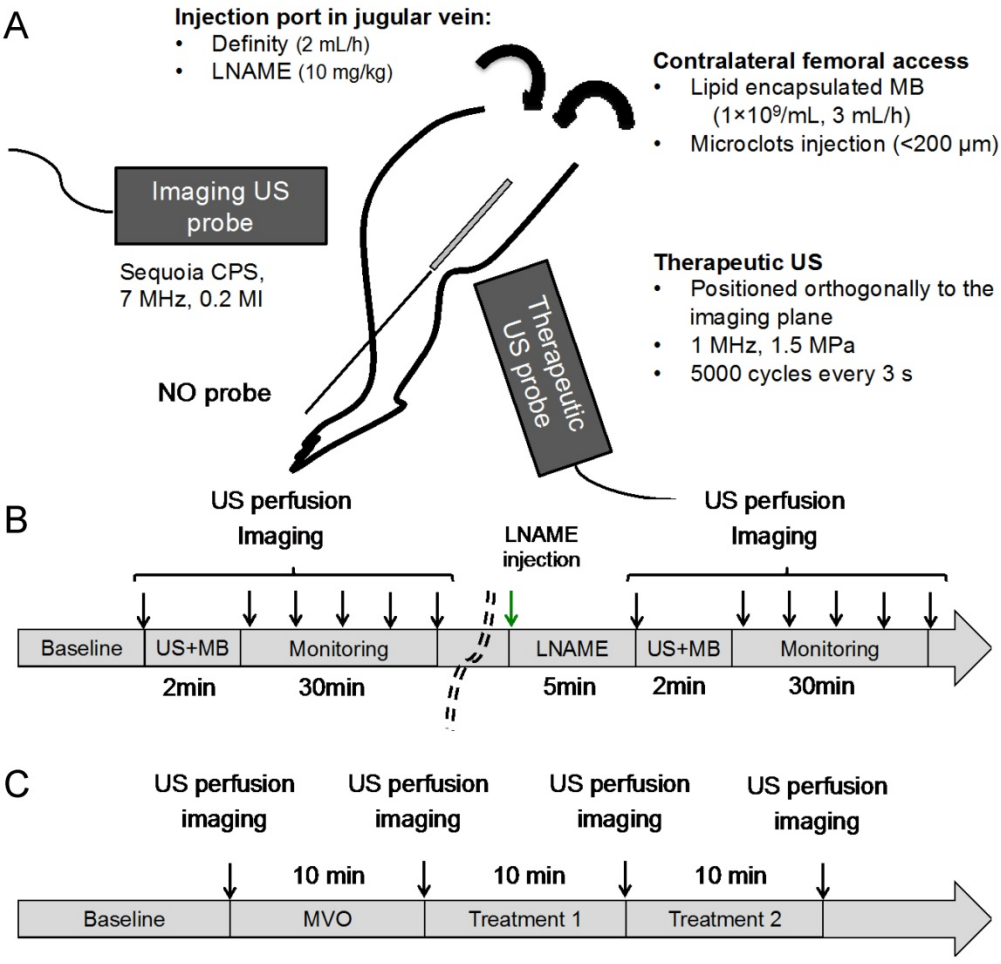

Figure 2: (A) *In vivo* hindlimb model for SRP therapy. Intramuscular NO was measured using a needle probe, microvascular perfusion was assessed using an imaging transducer and therapeutic US was delivered with a therapeutic transducer positioned perpendicularly to the imaging probe (more details on the probes orientations can be found in supplemental Figure S2; (B) The kinetics of NO and perfusion rate following SRP were assessed for 30 min after 2 min of SRP therapy with and without LNAME; (C) MVO was created by injecting microclots (See supplemental Figure S1). Two successive 10 min SRP therapy sessions were performed with and without LNAME.

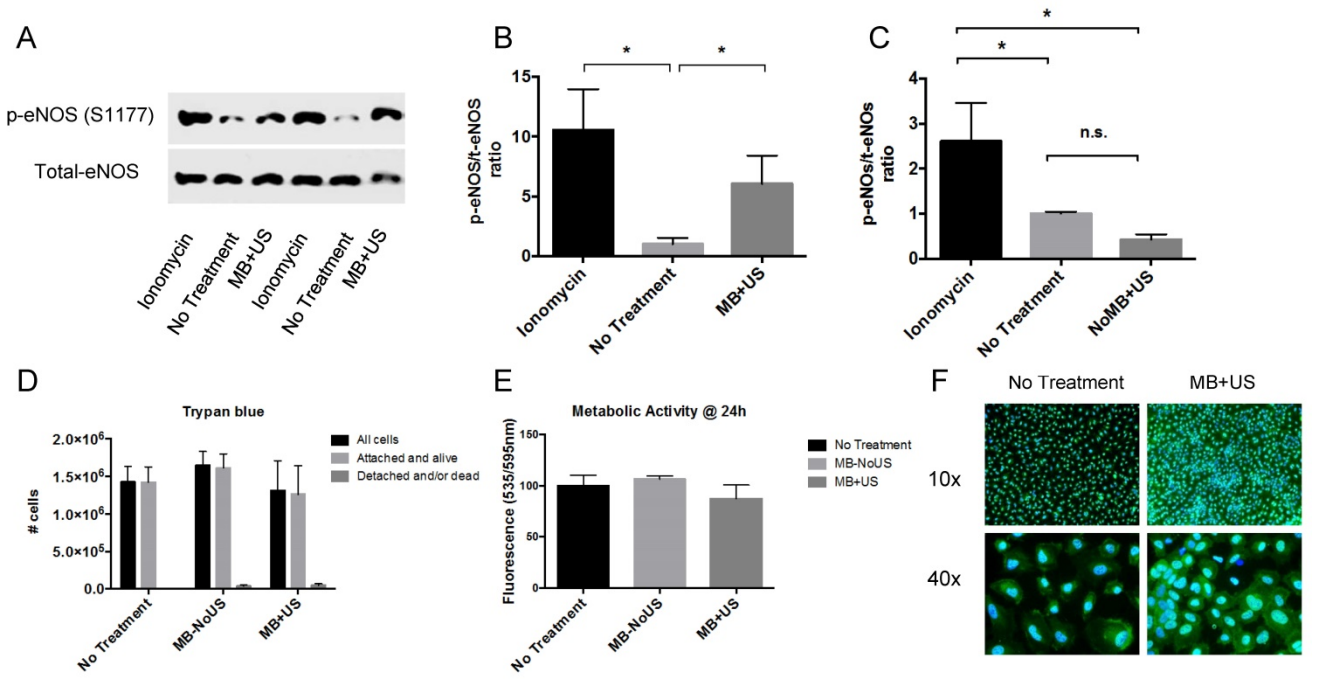

Figure 3: *In vitro* eNOS phosphorylation: (A) Western blot of phospho-eNOS (S1177) and total-eNOS for Ionomycin (+ control), No Treatment (- control) and MB+US therapy; p-eNOS/t-eNOS ratio increased following MB+US therapy (n=3); (B,C) p-eNOS/t-eNOS ratio without MB did not induce eNOS phosphorylation (n=3); (D) Trypan blue exclusion assay from supernatant and trypsinized cells and (E) metabolic activity measured by Alamar Blue fluorescence at 24 h, both showing that cells tolerated MB+US therapy; (F) immunostaining for p-eNOS (green) with Hoechst (blue) nuclear counter stain (* p<0.05)

Experimental protocol for microvascular obstruction model

Hindlimb ischemia from MVO (Figure 2C) was induced by injection of microthrombi into the femoral artery catheter until there was an estimated 75% decrease in peak video-intensity in the hindlimb, as monitored by simultaneous diagnostic US contrast perfusion imaging. The obstruction was maintained for 10 minutes prior to proceeding with US therapy. If spontaneous reperfusion occurred (brightness increased above the 25% threshold of peak videointensity), additional microthrombi were administered as needed to maintain 10 min of stable hypoperfusion. In 9 rats, L-NAME (10 mg/kg iv) was administered prior to microembolization to block endogenous endothelial NO production. Eight control rats did not receive L-NAME prior to microembolization. After 10 minutes of stable hypoperfusion, therapeutic US (5,000 cycles every 3 s at 1 MHz, 1.5 MPa) was delivered during simultaneous infusion of custom lipid MB into the femoral artery catheter via syringe pump at a flow rate of 3 mL/h. Two successive therapeutic SRP sessions of 10 minutes each were performed. Burst replenishment imaging during continuous intravenous infusion of Definity as described above was performed at baseline, after MVO, and after each of the 10 min SRP therapy sessions. Heart rate, respiration and O_2 saturation were continuously monitored. At the end of the experiment, animals were euthanized by isoflurane overdose and heart excision.

Statistics

All data were expressed as mean ± standard deviation. Comparisons were made using 2-way repeated measure ANOVA to compare the effects of treatment time and presence of LNAME. Multiple comparisons analysis to discern differences between groups was performed using Sidak's post-hoc testing. All tests were performed using Prism 6.0 (Graphpad software, LaJolla, CA). A p-value < 0.05 was considered statistically significant.

Results

Microbubble and ultrasound therapy causes phosphorylation of eNOS in plated endothelial cells

HUVECs exposed to MB+US had a marked increase in eNOS phosphorylation at serine 1177 (S1177) (Figure 3A) but total eNOS did not change, as expected. The ratio of p-eNOS/t-eNOS increased by 6-fold compared to the 'No Treatment' group (Figure 3B). eNOS phosphorylation did not occur upon US exposure without MB (Figure 3C), demonstrating that under the current US regime, MB oscillations are needed to induce eNOS phosphorylation. Trypan blue exclusion assay (Figure 3D) and Alamar Blue staining

(Figure 3E) at 24 h both supported that MB+US did not alter cell viability. We observed a decrease in cellular metabolic activity (Alamar Blue assay) immediately after exposure to MB+US (data not shown) but the cells fully recovered within 24 h. Immunostaining (Figure 3F) showed an increase in cytosolic fluorescence following MB+US exposure, consistent with eNOS translocation from the plasma membrane to the cytosol upon phosphorylation [23].

Hindlimb intramuscular NO

Next, we tested whether SRP could cause NO release *in vivo* in skeletal muscle using a needle NO probe. We first tested the effect of the LNAME injection on the intramuscular NO signal. We found that LNAME caused a sustained decrease in NO for > 55 min (Figure 4A), indicating sufficient eNOS inhibition for the duration of the experiment. To minimize variations in the NO signals caused by probe positioning (the probe position relative to feeding blood vessels or NO producing endothelial cells), the experiments with intact eNOS and impaired eNOS (LNAME) were performed sequentially in the same animals. We found that following 2 min of SRP treatment, intramuscular NO initially decreased below baseline at 3 and 5 min (p<0.05) before steadily increasing over the next 30 min, reaching a level above baseline 13 min after US (Figure 4B). This increase was completely blunted in the presence of LNAME and NO levels remained under baseline levels. The difference with and without LNAME became significantly different at t >13 min post SRP.

Typical frames from the burst reperfusion cineloops, taken 2 s after the burst frames, are shown in Figure 5A. The area highlighted in yellow marks the region receiving therapeutic ultrasound. It can be seen that within this region, videointensity initially decreased after ultrasound exposure, was partially restored at 3 min and increased above baseline at 6 min. To quantify these observations, regions of interest (ROI) were drawn encompassing the microcirculation, by excluding the feeding arteries, and ROI videointensity was measured throughout the cineloop burst replenishment sequence to measure microvascular blood volume (**MBV**) (Figure 5B) and perfusion rate (Figure 5C). While MBV was not significantly different following SRP, the flow rate increased significantly above baseline at 6 min and 10 min post SRP (p<0.05). At 30 min post SRP, there was a trend (p=0.07) toward increased perfusion rate compared to baseline. The increase in flow rate was abolished in the presence of LNAME. Typical cineloops at 10 min post SRP with and without LNAME can be found in supplemental videos 2 and 3. This increase in perfusion was found to be present for at least up to 4 h after MB+US therapy (See supplemental Figure S3).

Effect of LNAME on SRP

Physiologic Parameters

In the MVO experiment (Figure 2C), the rats received an average of 1.0 ± 0.4 mL of clot solution. Heart rate, respiration rate and O_2 saturation remained stable and within normal limits during the entire procedure. Following administration of microthrombi, the left rear paw became cyanotic, indicative of impaired perfusion. During reperfusion, the cyanosis resolved and the paw returned its baseline pink color in the SRP group but not in the group receiving LNAME (Figure 6).

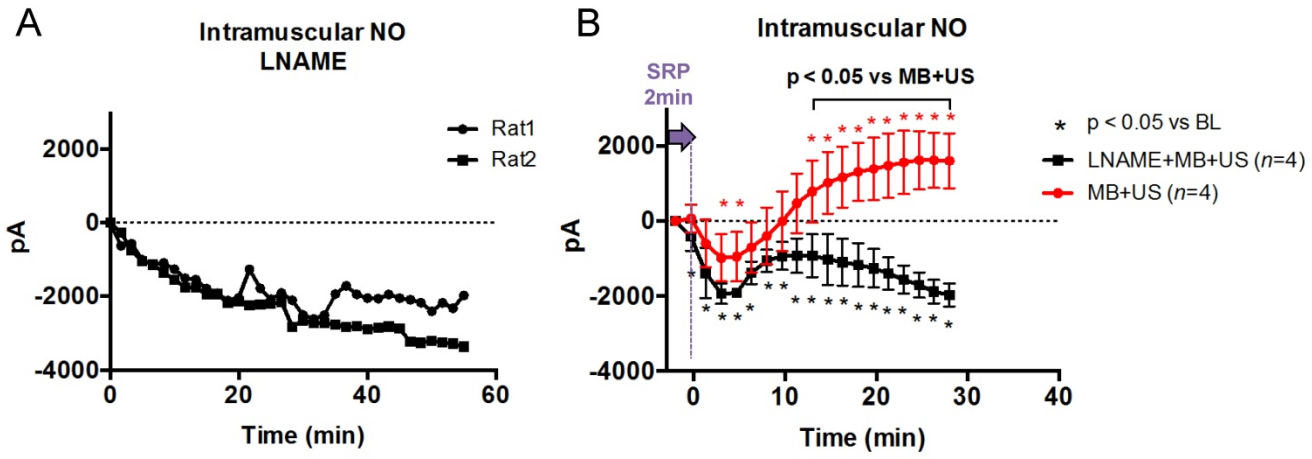

Figure 4: (A) Intramuscular NO after LNAME injection (No US): Intramuscular NO level decreased steadily following i.v. LNAME injection at t=0 s in two rats, as expected; (B) Intramuscular NO following SRP in 4 rats with and without LNAME. After a transient initial decrease, NO rose steadily following 2 min of SRP therapy and was significantly higher than at baseline starting 13 min after treatment. This increase was completely blunted with LNAME (Sidak's multiple comparison).

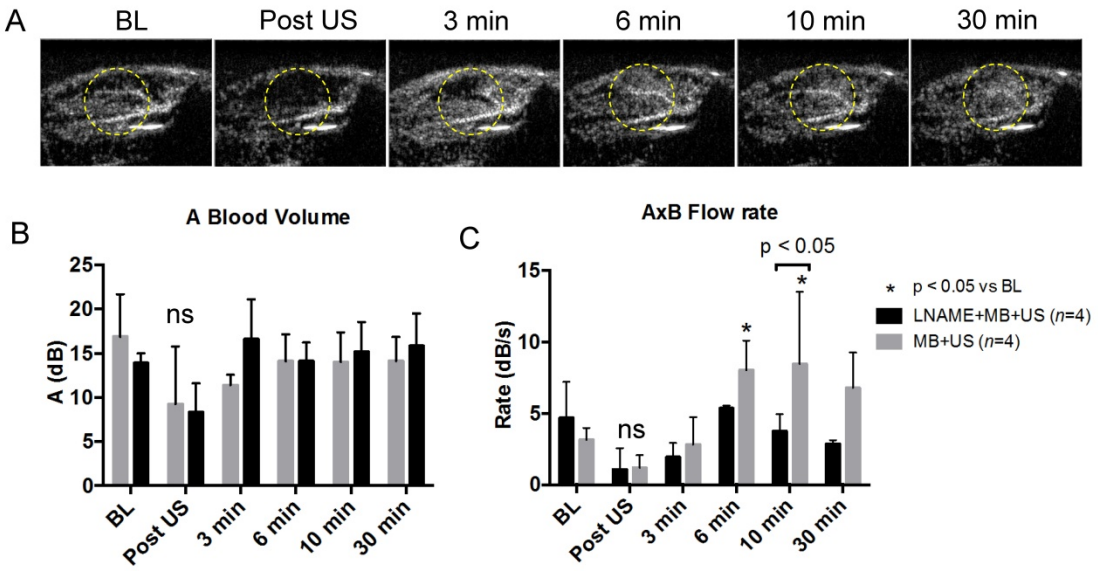

Figure 5: (A) Hindlimb contrast ultrasound imaging, in the MB+US group and without microthrombi, taken 2 s into the burst reperfusion imaging video sequence at baseline, post SRP (t=2 min) and at t=3, 6, 10 and 30 min. Note the transient decrease in echo contrast in the treated area (circle) after SRP followed by recovery at t=3 min and improved perfusion above baseline after 6 min; (B) Blood volume and (C) microvascular flow rate during and following 2 min of SRP therapy in rats receiving MB+US and LNAME+MB+US. Typical video sequences can be found in supplemental video data.

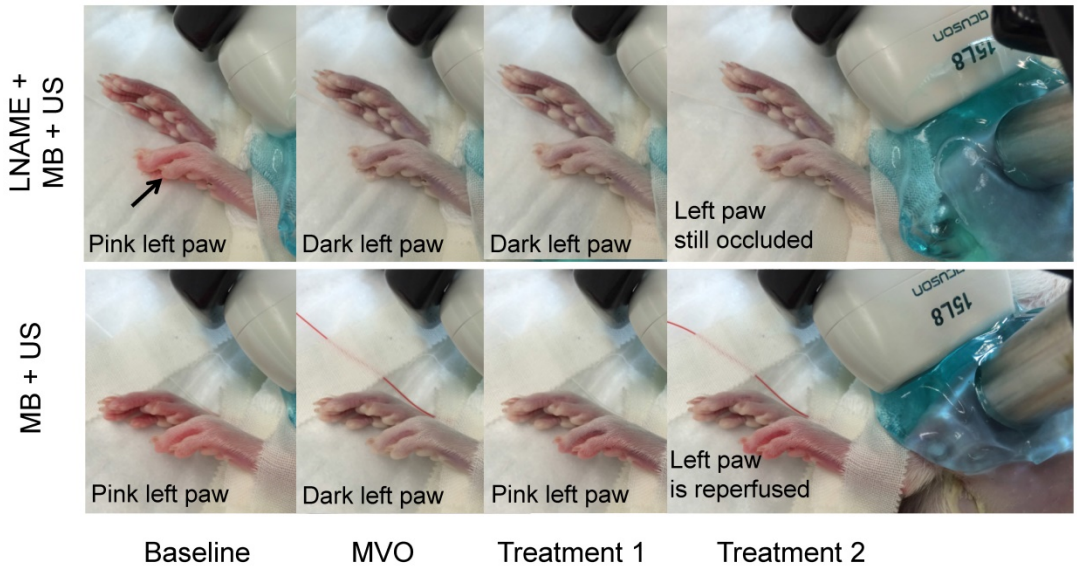

Figure 6: Photographs of rear paws taken at baseline, after MVO, and after two sessions of SRP therapy. In the LNAME+MB+US animal, the left paw, originally pink, becomes cyanotic after injection of microthrombi. It remains cyanotic after two sessions of SRP therapy. In the second row, in the MB+US group (intact NO), the paw returns to pink in color after the first SRP treatment and remains pink after treatment 2. The right paw, which becomes ischemic after placement of the catheter in the femoral artery and remains ischemic throughout, is shown for comparison.

Quantification of microvascular blood volume

In Figure 7, still frame contrast images of peak plateau video intensity, obtained 20 s after the burst are represented at baseline, after microvascular obstruction, after treatment 1, and after treatment 2 for the MB+US (intact eNOS) and L-NAME+MB+US (eNOS blockade) groups.

Video intensity, reflecting MB concentration in the imaged tissue (intramuscular microvascular cross sectional area or MBV), was significantly decreased during microvascular obstruction and restored toward baseline after 2 sessions of SRP therapy. However, in the animals that received L-NAME to block NO production, reperfusion was significantly impaired (reduced MBV) compared to controls (intact NO).

To quantify these observations, we created regions of interest (ROI) encompassing the microcirculation, by excluding the feeding arteries and measured ROI videointensity throughout the cine loop burst replenishment sequence to measure MBV and perfusion rate. Administration of microthrombi had a significant effect on MBV (p<0.001 vs baseline), reducing MBV by more than 85% in both groups (Figure 8).

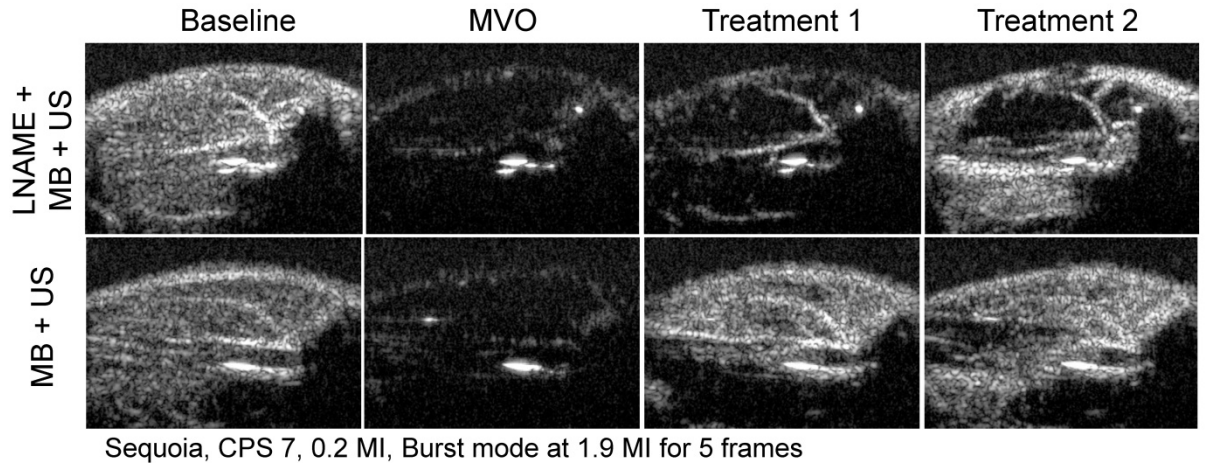

Figure 7: Contrast enhanced ultrasound images, taken 20 s after burst, for baseline, MVO and SRP treatments 1 and 2 for a rat in the LNAME + MB + US and MB + US groups. Reperfusion is near complete after SRP therapy in the MB + US rat, but not in the rat with NO blockade by LNAME.

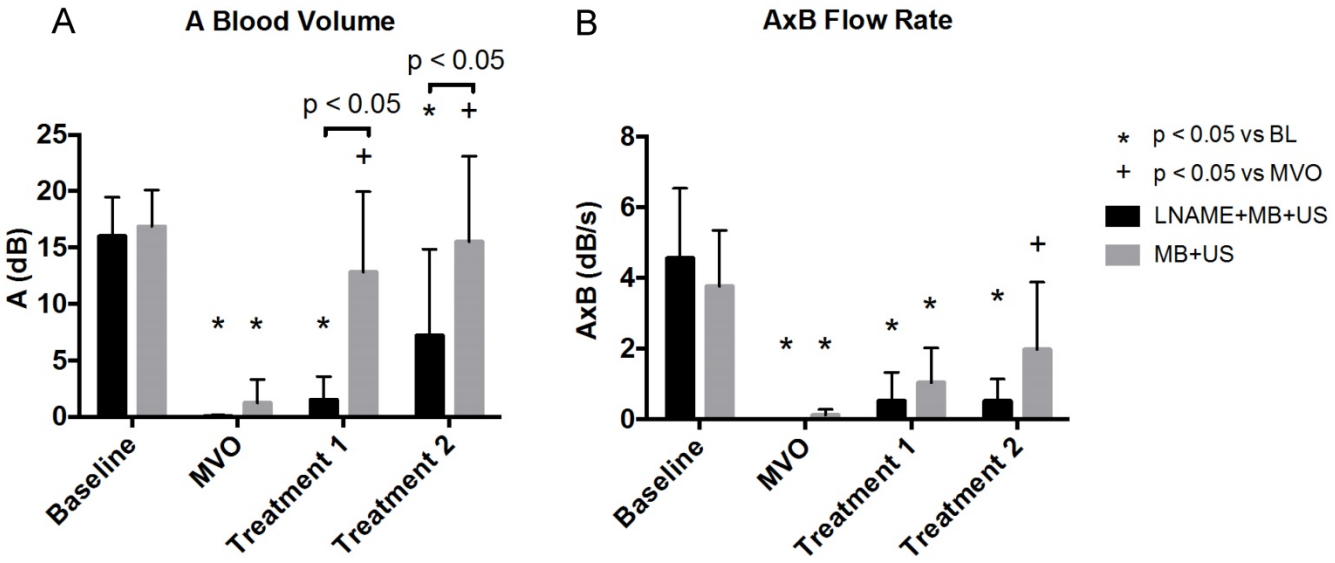

Figure 8: Blood volume and flow rate calculated using contrast enhanced burst replenishment ultrasound imaging at different stages of sonoreperfusion therapy using MB+US with LNAME (*n*=9) and without LNAME (*n*=9).

After US treatment 1, MBV was restored to baseline in the MB+US control group (12.8 ± 7.2 dB, $p<0.05$ vs MVO stage). However, during blockade of endothelial NO production with LNAME, MBV remained low (1.5 ± 2.1 dB), indicating persistent hypoperfusion. After US treatment 2, MBV remained at baseline levels (16.9 ± 3.3 dB) in the MB+US control group. However, in the MB+US+LNAME rats, MBV remained statistically unchanged from the MVO stage. LNAME did not have an effect on the perfusion rate (AxB) (p=n.s., data not shown). The flow rate was significantly impaired in both groups following microthrombi injection. In the MB+US group, there was a numerical increase in flow rate compared to MVO stage after treatment 1, that became statistically significantly greater compared to MVO stage after treatment 2 (2.0 ± 1.9 dB), whereas, in the LNAME animals, the flow rate remained blunted after both treatment sessions.

Discussion

We have previously demonstrated that sonoreperfusion (SRP) therapy can restore microvascular perfusion in both *in vitro* and *in vivo* models of microvascular obstruction (MVO) [15, 16]. In the present study, we build upon this work by exploring a potentially important biological response of SRP therapy, and tested the hypothesis that nitric oxide (NO) plays a significant role in SRP efficacy, owing to the unique interactions between microbubbles and ultrasound, and the consequent effect on endothelium. Although there has been

primary focus on the direct mechanical consequences of MB cavitation on thrombi during SRP [17], the independent biological effects of MB vibrations on the shear-sensitive vascular endothelium bear consideration.

During rat hindlimb tourniquet ischemia [24] or LAD occlusion in canines [25], 27 kHz US (no MBs) was shown to improve perfusion through generation of NO. Similarly, it was found that exposure to 9 min of continuous wave ultrasound over several days could activate the PI3K-Akt-eNOS in mice [26, 27]. These studies were conducted without MBs and using high duty cycle US (30-100% duty cycle), in contrast to our work, in which MB oscillations in response to 1 MHz US were induced intravascularly in the microcirculation using pulsed ultrasound with low duty cycle (<0.16% duty cycle) and thus excluding any thermal effects. Oscillating MBs impart shear stress on the surrounding medium, the effects of which could be more pronounced in the microcirculation, where the MB to vessel diameter ratio is large, and which could include endothelial mechanotransduction and NO release. We first tested this hypothesis *in vitro* by exposing HUVEC cell cultures and found that SRP could induce eNOS phosphorylation at serine S1177, which is known to be a major pathway for endothelial NO production. The magnitude of shear required to generate endothelial NO is 3-9 Pa [28], well within the range of shear generated by acoustic microstreaming [29]. Changing shear force on the vascular endothelium stimulates endothelial cell NO release through eNOS within seconds [20]. NO is not only a potent vasodilator but also affects other components of MVO [20]: platelet aggregation, increased adhesion of inflammatory cells and vasoconstriction are all attenuated by NO, potentially lending multifactorial therapeutic mechanisms to the MB+US efficacy.

We then investigated if endothelial NO could be released by SRP *in vivo* in an intact hindlimb with normal endothelium (No MVO). We used our previously described rat hindlimb model, and measured intramuscular NO in an intact skeletal muscle treated with 2 min of SRP therapy. It was found that following a transient delay, intramuscular NO rose continuously starting 5 min post treatment and was maintained up to 30 min post treatment. This increase in NO was associated with an increase in microvascular blood flow rate above baseline level at 6 and 10 min post treatment, which was consistent with NO mediated vasodilation. The increases of both intramuscular NO and flow rate following SRP were blunted with endothelial eNOS blockade using LNAME, demonstrating that SRP causes sustained NO-mediated improvements in microvascular perfusion that can last at least 30 min following therapeutic US. To our knowledge, this is the first report quantifying the time course of improved microcirculatory perfusion following SRP therapy and the first demonstration of a sustained improvement in NO release and perfusion indices occurring after cessation of SRP therapy.

Finally, in this study, we tested the contribution of NO to SRP by administering LNAME prior to SRP therapy in our rat hindlimb model of MVO. This intact skeletal muscle model of MVO provides an excellent opportunity to explore both the mechanical and biological mechanisms of SRP, in contrast to our previous *in vitro* study in which we explored the isolated mechanical effects of SRP and demonstrated its reperfusion efficacy [16]. Using US contrast perfusion imaging, our aggregated results indicate that two sessions of SRP therapy improved blood volume and mean flow rate in the microcirculation (Figures 7 and 8). These findings were corroborated by the reversal of visually observable limb cyanosis in the treated rats (Figure 6). In all cases, the reperfusion efficacy was reduced in the presence of eNOS-blockade with LNAME. For instance, blood volume was restored to baseline level after two successive rounds of SRP therapy in the MB+US group but not in the LNAME+MB+US group, in which blood volume remained significantly reduced from baseline (Figure 8). However, blood volumes continued to increase in both groups after treatment 2, consistently with additive therapeutic efficacy of longer treatment times, but the blunting effect of LNAME on blood volume restoration was still significant after treatment 2 (p<0.05). The flow rate also increased in the MB+US group after Treatment 2, whereas the flow rate remained blunted after both treatment sessions during blockade of eNOS with LNAME. Overall, during blockade of endothelial NO production with LNAME, we found that restoration of microvascular blood volume during SRP therapy was incomplete, thus confirming our hypothesis that NO plays a significant role in the SRP efficacy. Importantly, NO blockade did not completely abrogate the effects of SRP, and restored partial reperfusion in the LNAME-treated rats, suggesting that SRP efficacy is not solely NO dependent, and that other biological or mechanical mechanisms are likely involved. Our data suggest that the interaction of the MB and the endothelium during application of US results in NO release, consistent with previous *in vitro* and non-ischemic *in vivo* models [24, 25, 30, 31]. Belcik et al. [32], recently reported that MB+US increased hindlimb perfusion rate in mice after 10 min of pulsed MB+US therapy and that the effect was attenuated during blockade of eNOS with LNAME. This group

also described an increase in flow rate in a model of chronic ischemia three days after MB+US therapy. Recently, it was shown that MB and ultrasound induced increase in blood flow was mediated by adenosine triphosphate (ATP) and purinergic signaling [33], which can stimulate the eNOS and/or adenosine and prostanoid pathways. Consistent with our findings, this study also found that LNAME blunted the blood flow increase observed after MB+US treatment. However, our work is distinct in that we specifically applied SRP therapy using a model of microvascular obstruction, where we created microthrombi to mechanically obstruct the microvasculature, versus the use of simple tourniquet ischemia. Our work is also unique in the sense that we use MB+US using long tone bursts (5,000 cycles) in our hindlimb model, and demonstrated the role of NO in the efficacy for treating MVO, as occurs clinically during acute myocardial infarction, stroke and peripheral vascular intervention. Our study demonstrates that long tone burst ultrasound with MB are efficacious for restoring flow during MVO and uncovers the important role of NO in mediating this effect. However, at this stage, it is difficult to fully assess the importance of NO-mediated effects against mechanical thrombus dissolution in SRP efficacy because both mechanisms may not be independent. If one assumes (1) that LNAME completely blocked NO and (2) that NO was the only biologically relevant (non mechanical) contributor to SRP, the data from Figure 8 would indicate that 12% and 49% of the increase in blood volume was caused by mechanical dissolution respectively following Tx1 and Tx2. By subtracting microvascular blood volume for the LNAME animals from the control animals, the NO pathway could then be attributed a major role (>50%) in the observed SRP efficacy. These assumptions and calculations are evidently simplistic in nature and do not account for interaction between the two pathways. The overarching conclusion from these data should be that both NO and mechanical dissolution both play a role in the observed SRP efficacy. Our findings are in line with the findings of a recent clinical trial [34], which showed that adjunct MB+US therapy prior to and following PCI in patients presenting with a first STEMI, not only improved angiographic recanalization prior to PCI, but also decreased the proportion of obstructed microvascular segments and improved ejection fraction at 1 month. This study demonstrated the clinical potential of short pulse high mechanical index MB+US as an adjunct therapy for patients presenting with STEMI. Moreover, in this study, the authors suggest that bioeffects other than mechanical thrombus dissolution may be responsible for the observed therapeutic effects. In our work presented herein, we clearly establish a role for NO using long tone burst ultrasound. At this point, the benefits and safety of longer ultrasound pulse length on the therapeutic efficacy of the approach remain to be established clinically. Our group and others have been investigating the use of longer tone burst to achieve sonothrombolysis, which demonstrated improved efficacy with longer pulses in preclinical studies [15, 16, 35, 36]. However, a small phase-2 clinical trial [37] using longer tone burst ultrasound (20 μs) was aborted prematurely (6 patients were enrolled) after the angiographic observation of vasoconstriction in three patients following MB+US therapy. It is important to note that all patients responded well to PCI after the transient vasoconstriction incident. Moreover, multiple confounding factors may contribute to vasoconstriction during PCI, including the milieu of acute myocardial infarction itself [38, 39]. In our experiments with long tone burst ultrasound (5,000 μs), we did observe a several minute delay in microvascular reperfusion following SRP therapy, which in the intact hindlimb was restored and returned to levels above baseline perfusion after 5 min. This transient episode of microvascular hypoperfusion occurring immediately after US therapy raises the possibility of microvascular vasoconstriction as an etiology. But further confirmatory studies will be required.

Limitations

In this study, we used high MI, long tone burst US parameters during SRP, as these setting generated the greatest efficacy *in vitro* [16], where we solely tested the mechanical effects of SRP. However, it was reported in a pig model of acute coronary syndrome [40] that MB+US using shorter pulses (up to 20 μs) could restore epicardial patency in up to 53% of cases and cause microvascular recovery with ST-segment resolution in up to 80% of animals. This was accomplished using a clinical scanner, with much shorter tone bursts, highlighting the fact that the US parameters required to achieve optimal SRP have yet to be determined. Further, the US parameters required to specifically optimize the NO component of SRP remain unknown, and require further exploration.

The volume concentration of microthrombi which we injected to cause microvascular obstruction was based on a worst-case scenario (i.e. large thromboembolic burden) causing a large hindlimb perfusion defect. In the clinical setting, the volume of microemboli would be more variable and would include atherosclerotic plaque components as well, both of which may affect the required US parameters

to achieve optimal SRP. Nonetheless, our rat model of microembolization is, to our knowledge, the closest *in vivo* replicant of MVO and serves as a useful, if simple, platform upon which testing fundamental mechanisms of SRP is possible.

The hemodynamic effect of LNAME causes an increase in vascular resistance, and we cannot exclude this as contributing to blunting of US/MB effect. However, the consequences of eNOS blockade will always result in hemodynamic changes and it is not possible to eliminate this effect under normal physiological conditions. Also, LNAME is not specific for inhibition of endothelial NO synthase alone. Therefore we cannot exclude the effects of other forms of NO synthase (iNOS, nNOS) on modulating NO and playing a role in SRP efficacy.

Finally, the microbubbles were injected intra-arterially in the hindlimb feeding vessel in this study, in contrast to other sonothrombolysis studies where MB were given intravenously. This maximized local microbubble delivery and minimized systemic dosing. For intravenous microbubble delivery, we would expect similar results but this may require adjusting MB dose.

Conclusions

These data suggest that SRP is effective in reestablishing microvascular perfusion in the setting of MVO and that NO plays a significant mechanistic role. This new understanding could inform strategies to tune SRP US regimes for optimal reperfusion of MVO following acute myocardial infarction.

Abbreviations

AMI: Acute myocardial infarction; CHD: Coronary heart disease; CPS: Contrast Pulse Sequence; LAD: Left Anterior Descending artery; LNAME: N-Nitro-L-Arginine Methyl Ester; MB: Microbubble; MI: mechanical index; MBV: Microvascular Blood Volume; MVO: Microvascular obstruction; NO: Nitric oxide; PFC: Perfluorocarbon; PCI: Percutaneous coronary intervention; SRP: Sonoreperfusion; US: Ultrasound

Supplementary Material

Supplemental video 1.
http://www.thno.org/v07p3527s1.avi
Supplemental video 2.
http://www.thno.org/v07p3527s2.avi
Supplemental video 3.
http://www.thno.org/v07p3527s3.avi
Supplemental video 4.
http://www.thno.org/v07p3527s4.mov
Supplemental figures.
http://www.thno.org/v07p3527s5.pdf

Acknowledgements

We thank Dr Flordeliza Villanueva for her sustained guidance and support, and Linda Lavery for her work in performing all surgical manipulations and preparing the experimental setup. The work was funded in part through the Dean's Bridge Fund Program of the University of Pittsburgh and the National Institutes of Health R01 HL125777 and R01 HL112904-02. Dr Adam Straub was funded by NIH R01 HL133864 and NIH R01 HL128304. There are no relationships with industry to disclose.

Author Contributions

Conception and design: FY, XC, AS, JP
Development of Methodology: FY, XC, JP
Acquisition of data: FY, XC
Analysis and interpretation of results: FY, XC, JP
Writing, review, and/or revision of the manuscript: FY, XC, AS, JP.

Competing Interests

The authors have declared that no competing interest exists.

References

1. Go AS, Mozaffarian D, Roger VL, Benjamin EJ, Berry JD, Borden WB, et al. Heart disease and stroke statistics--2013 update: a report from the American Heart Association. Circulation. 2013; 127: e6-e245.
2. Ito H, Maruyama A, Iwakura K, Takiuchi S, Masuyama T, Hori M, et al. Clinical implications of the 'no reflow' phenomenon. A predictor of complications and left ventricular remodeling in reperfused anterior wall myocardial infarction. Circulation. 1996; 93: 223-8.
3. Wu KC, Zerhouni EA, Judd RM, Lugo-Olivieri CH, Barouch LA, Schulman SP, et al. Prognostic significance of microvascular obstruction by magnetic resonance imaging in patients with acute myocardial infarction. Circulation. 1998; 97: 765-72.
4. Costantini CO, Stone GW, Mehran R, Aymong E, Grines CL, Cox DA, et al. Frequency, correlates, and clinical implications of myocardial perfusion after primary angioplasty and stenting, with and without glycoprotein IIb/IIIa inhibition, in acute myocardial infarction. J Am Coll Cardiol 2004; 44: 305-12.
5. Tanaka A, Imanishi T, Kitabata H, Kubo T, Takarada S, Tanimoto T, et al. Lipid-rich plaque and myocardial perfusion after successful stenting in patients with non-ST-segment elevation acute coronary syndrome: an optical coherence tomography study. Eur Heart J. 2009; 30: 1348-55.
6. Montorsi P, Caputi L, Galli S, Ciceri E, Ballerini G, Agrifoglio M, et al. Microembolization during carotid artery stenting in patients with high-risk, lipid-rich plaque. A randomized trial of proximal versus distal cerebral protection. J Am Coll Cardiol. 2011; 58: 1656-63.
7. Prasad A, Herrmann J. Myocardial infarction due to percutaneous coronary intervention. N Engl J Med. 2011; 364: 453-64.
8. Goldstein JA, Maini B, Dixon SR, Brilakis ES, Grines CL, Rizik DG, et al. Detection of lipid-core plaques by intracoronary near-infrared spectroscopy identifies high risk of periprocedural myocardial infarction. Circ Cardiovasc Interv 2011; 4: 429-37.
9. Isshiki T, Kozuma K, Kyono H, Suzuki N, Yokoyama N, Yamamoto Y. Initial clinical experience with distal embolic protection using "Filtrap", a novel filter device with a self-expandable spiral basket in patients undergoing percutaneous coronary intervention. Cardiovasc Interv Ther. 2011; 26: 12-7.
10. Khumri TM, Nayyar S, Idupulapati M, Magalski A, Stoner CN, Kusnetzky LL, et al. Usefulness of myocardial contrast echocardiography in predicting late mortality in patients with anterior wall acute myocardial infarction. Am J Cardiol. 2006; 98: 1150-5.
11. Gibson CM. Has my patient achieved adequate myocardial reperfusion? Circulation. 2003; 108: 504-7.
12. Jaffe R, Dick A, Strauss BH. Prevention and treatment of microvascular obstruction-related myocardial injury and coronary no-reflow following percutaneous coronary intervention: a systematic approach. JACC Cardiovasc Interv. 2010; 3: 695-704.
13. Mauri L, Rogers C, Baim DS. Devices for distal protection during percutaneous coronary revascularization. Circulation. 2006; 113: 2651-6.

14. Porto I, Biasucci LM, De Maria GL, Leone AM, Niccoli G, Burzotta F, et al. Intracoronary microparticles and microvascular obstruction in patients with ST elevation myocardial infarction undergoing primary percutaneous intervention. Eur Heart J. 2012; 33: 2928-38.
15. Pacella JJ, Brands J, Schnatz FG, Black JJ, Chen X, Villanueva FS. Treatment of microvascular micro-embolization using microbubbles and long-tone-burst ultrasound: an *in vivo* study. Ultrasound Med Biol. 2015; 41: 456-64.
16. Leeman JE, Kim JS, Yu FT, Chen X, Kim K, Wang J, et al. Effect of acoustic conditions on microbubble-mediated microvascular sonothrombolysis. Ultrasound Med Biol. 2012; 38: 1589-98.
17. Chen X, Leeman JE, Wang J, Pacella JJ, Villanueva FS. New insights into mechanisms of sonothrombolysis using ultra-high-speed imaging. Ultrasound Med Biol. 2014; 40: 258-62.
18. Helfield B, Chen X, Watkins SC, Villanueva FS. Biophysical insight into mechanisms of sonoporation. Proc Natl Acad Sci U S A. 2016; 113: 9983-8.
19. Furchgott RF, Zawadzki JV. The obligatory role of endothelial cells in the relaxation of arterial smooth muscle by acetylcholine. Nature. 1980; 288: 373-6.
20. White CR, Frangos JA. The shear stress of it all: the cell membrane and mechanochemical transduction. Philos Trans R Soc Lond B Biol Sci. 2007; 362: 1459-67.
21. Weller GE, Villanueva FS, Klibanov AL, Wagner WR. Modulating targeted adhesion of an ultrasound contrast agent to dysfunctional endothelium. Ann Biomed Eng. 2002; 30: 1012-9.
22. Wei K, Jayaweera AR, Firoozan S, Linka A, Skyba DM, Kaul S. Quantification of myocardial blood flow with ultrasound-induced destruction of microbubbles administered as a constant venous infusion. Circulation. 1998; 97: 473-83.
23. Figueroa XF, Gonzalez DR, Puebla M, Acevedo JP, Rojas-Libano D, Duran WN, et al. Coordinated endothelial nitric oxide synthase activation by translocation and phosphorylation determines flow-induced nitric oxide production in resistance vessels. J Vasc Res. 2013; 50: 498-511.
24. Suchkova VN, Baggs RB, Sahni SK, Francis CW. Ultrasound improves tissue perfusion in ischemic tissue through a nitric oxide dependent mechanism. Thromb Haemost. 2002; 88: 865-70.
25. Siegel RJ, Suchkova VN, Miyamoto T, Luo H, Baggs RB, Neuman Y, et al. Ultrasound energy improves myocardial perfusion in the presence of coronary occlusion. J Am Coll Cardiol. 2004; 44: 1454-8.
26. Lu ZY, Li RL, Zhou HS, Huang JJ, Su ZX, Qi J, et al. Therapeutic ultrasound reverses peripheral ischemia in type 2 diabetic mice through PI3K-Akt-eNOS pathway. Am J Transl Res. 2016; 8: 3666-77.
27. Huang JJ, Shi YQ, Li RL, Hu A, Lu ZY, Weng L, et al. Angiogenesis effect of therapeutic ultrasound on HUVECs through activation of the PI3K-Akt-eNOS signal pathway. Am J Transl Res. 2015; 7: 1106-15.
28. Ziegler T, Silacci P, Harrison VJ, Hayoz D. Nitric oxide synthase expression in endothelial cells exposed to mechanical forces. Hypertension. 1998; 32: 351-5.
29. Doinikov AA, Bouakaz A. Theoretical investigation of shear stress generated by a contrast microbubble on the cell membrane as a mechanism for sonoporation. J Acoust Soc Am. 2010; 128: 11-9.
30. Wu J, Nyborg WL. Ultrasound, cavitation bubbles and their interaction with cells. Adv Drug Deliv Rev. 2008; 60: 1103-16.
31. Davis CM, Ammi AY, Alkayed NJ, Kaul S. Ultrasound stimulates formation and release of vasoactive compounds in brain endothelial cells. Am J Physiol Heart Circ Physiol. 2015; 309: H583-91.
32. Belcik JT, Mott BH, Xie A, Zhao Y, Kim S, Lindner NJ, et al. Augmentation of limb perfusion and reversal of tissue ischemia produced by ultrasound-mediated microbubble cavitation. Circ Cardiovasc Imaging. 2015; 8.
33. Belcik JT, Davidson BP, Xie A, Wu MD, Yadava M, Qi Y, et al. Augmentation of Muscle Blood Flow by Ultrasound Cavitation Is Mediated by ATP and Purinergic Signaling. Circulation. 2017; 135: 1240-52.
34. Mathias W, Jr., Tsutsui JM, Tavares BG, Xie F, Aguiar MO, Garcia DR, et al. Diagnostic Ultrasound Impulses Improve Microvascular Flow in Patients With STEMI Receiving Intravenous Microbubbles. J Am Coll Cardiol. 2016; 67: 2506-15.
35. Wu J, Xie F, Kumar T, Liu J, Lof J, Shi W, et al. Improved sonothrombolysis from a modified diagnostic transducer delivering impulses containing a longer pulse duration. Ultrasound Med Biol. 2014; 40: 1545-53.
36. Porter TR, Radio S, Lof J, Everbach C, Powers JE, Vignon F, et al. Diagnostic Ultrasound High Mechanical Index Impulses Restore Microvascular Flow in Peripheral Arterial Thromboembolism. Ultrasound Med Biol. 2016; 42: 1531-40.
37. Roos ST, Juffermans LJ, van Royen N, van Rossum AC, Xie F, Appelman Y, et al. Unexpected High Incidence of Coronary Vasoconstriction in the Reduction of Microvascular Injury Using Sonolysis (ROMIUS) Trial. Ultrasound Med Biol. 2016; 42: 1919-28.
38. Sahin M, Demir S, Kocabay G, Bulut M, Alici G, Ozkan B, et al. Coronary vessel diameters during and after primary percutaneous coronary artery intervention. Herz. 2014; 39: 515-21.
39. Oliva PB, Breckinridge JC. Arteriographic evidence of coronary arterial spasm in acute myocardial infarction. Circulation. 1977; 56: 366-74.
40. Xie F, Lof J, Matsunaga T, Zutshi R, Porter TR. Diagnostic ultrasound combined with glycoprotein IIb/IIIa-targeted microbubbles improves microvascular recovery after acute coronary thrombotic occlusions. Circulation. 2009; 119: 1378-85.